Photocatalytic degradation of methylparathion - an endocrine disruptor by Bi^{3+}-doped TiO$_2$

S. Rengaraj[1], X.Z. Li[*1], P.A. Tanner[2], Z. Pan[2], G.K.H. Pang[3]

[1] *Department of Civil and Structural Engineering,*
The Hong Kong Polytechnic University, Hong Kong S.A.R., P.R. China
[2] *Department of Chemistry and Biology,*
City University of Hong Kong, Hong Kong S.A.R., P.R. China
[3] *Department of Applied Physics,*
The Hong Kong Polytechnic University, Hong Kong S.A.R., P.R. China

Abstract

The relationships between the catalyst physicochemical properties and its photocatalytic activity have been investigated and elucidated in the photodegradation of the organophosphate insecticide methylparathion. The photocatalytic degradation was investigated by using a sol-gel synthesized Bi^{3+}-doped TiO$_2$ nanocatalyst (using doping concentrations up to 2 wt% Bi^{3+}) under UV-A light in aqueous suspension. The prepared photocatalysts were characterized by X-ray diffraction, (environmental) scanning electron microscopy, transmission electron microscopy, energy dispersive X-ray analysis, IR-UV-visible absorption spectra, X-ray photoelectron emission spectroscopy and room- and low- temperature photoluminescence spectra. The photodegradation and mineralization products of methylparathion were analyzed by high performance liquid chromatography, dissolved organic carbon and ion chromatography techniques. The experiments demonstrated that the presence of Bi^{3+} in TiO$_2$ catalysts substantially enhances the photocatalytic degradation of methylparathion in aqueous suspension. The degradation of methylparathion by these catalysts followed a first-order kinetic model and an optimal dosage between 0.7% and 1.5% Bi^{3+} in TiO$_2$ achieved the fastest methylparathion degradation under the experimental conditions. This study has also investigated the mineralization of methylparathion in terms of carbon, sulphur and nitrogen conversion during the photocatlaytic reaction. The possible mechanisms of photoluminescence quenching and photodegradation are elucidated in the context of donor-acceptor interactions with Bi-O polyhedra acting as electron trapping centres which hinder electron-hole pair recombination.

---

[*] Corresponding author. Tel.: +852 2766 6016; fax: +852 2334 6389; E-mail address: cexzli@polyu.edu.hk (X.Z. Li).

1.   Introduction

Endocrine disrupting chemicals (EDCs) have been shown to produce changes in the endocrine system of organism that may lead to increase in cancers and abnormalities in reproductive structure and function. Recent research has highlighted the existence of hormonally active compounds in sewage and industrial effluents and their potential for recycling back into the environment including drinking water supplied through point and non-point sources. On the other hand, surplus pesticides, even though within their expiration limits, will become a burden when their future use is prohibited by legislation due to toxicological or environmental concerns. Furthermore, the Food and Agricultural Organization of the United Nations (FAO) has estimated that more than 400 kilotonnes of obsolete pesticides are stocked worldwide [1,2]. The disposal of EDCs such as pesticides, fungicides and insecticides can cause serious environmental problems due to the chemical toxicity of the active ingredients in the formulations and sometimes, of their decomposition products.

Methylparathion is one of the most widely-used organophosphate insecticides. Its widespread use has caused environmental concern due to its frequent leakage into surface and ground waters. It is acutely toxic to mammals, for example the oral LD$_{50}$ for rats is in the range 18-50 mg kg^{-1}. It acts by inhibiting the enzyme acetyl cholinesterase in nerve tissue. An ideal treatment method for such pesticide wastes should be non-selective, achieve rapid and complete degradation to inorganic products and be suitable for small-scale wastes. Possible methods include biodegradation, chemical reaction, physical entrainment, and incineration. Entrainment is losing acceptance as a final solution for waste disposal. Incineration is prohibitively expensive for dilute aqueous wastes because of high-energy requirements and transport costs. Biodegradation and chemical reaction, especially oxidative photodegradation, look to be the most promising methods.

Various innovative technologies have been proposed for methylparathion treatment. These include the use of UV radiation and hydrogen peroxide [3,4], ultrasonic irradiation [5], or mercury promoted hydrolysis [6]. The major disadvantage of these technologies is that they are designed for decontamination of aqueous solutions with very low active ingredient contents and are not suitable for degrading higher concentrations of unwanted pesticides. Furthermore, the use of mercury species is to be discouraged. Among various oxide semiconductor photocatalysts, TiO_2 is known as one of the most effective for the degradation of organic pollutants and its photocatalytic behavior has been studied extensively [7,8]. Although TiO_2 catalysts are capable of decomposing a wide variety of organic and inorganic pollutants and toxic materials in both liquid and gas phase systems [9,10], the fast recombination rate of photogenerated electron-hole pairs prevents the commercialization of this technology. For this reason, much attention has been paid to doping the material with transition and noble metals. The presence of heavy metals, such as Pt, Pd, Au and Ag has been demonstrated to enhance the degradation efficiency of photocatalytic reactions [11,12].

The present work focuses on the preparation, characterization and application of Bi^{3+}-doped TiO_2 photocatalysts (hereafter referred to as $Bi-TiO_2$) for the degradation of the environmental EDC methylparathion: $(H_3C-O)_2P(=S)-O-C_6H_4NO_2$. Not only has the photodegradation efficiency shown an improvement relative to that for the undoped photocatalyst, but some understanding of the mechanisms of photoluminescence and photodegradation have been forthcoming. The experimental details are presented in Section 2. In Section 3 the characterizations of the photocatalysts using different instrumental techniques are described. The results from the photodegradation study are presented in Section 4 and some conclusions are listed in Section 5.

2. Experimental

2.1. Materials

Titanium tetra-n-butoxide $(Ti(O-Bu)_4)$ and bismuth nitrate (both AR analytical grade, Aldrich Chemical Company, USA) were used as titanium and bismuth sources for the preparation of TiO_2 and $Bi-TiO_2$ photocatalysts. Methylparathion was obtained from the Pesticide Testing Laboratory, Tamil Nadu Agricultural University, India (AR grade) and used

without further purification. Deionised, doubly distilled water was used for the preparation of all solutions. Water and acetonitrile (International Laboratory, USA - HPLC-grade) were used as HPLC eluents.

2.2. Preparation of photocatalysts

The bismuth doped TiO_2 samples (Bi-TiO_2) were prepared by the sol-gel method in which 21 ml of $Ti(O-Bu)_4$ was dissolved in 80 ml of absolute ethanol, and the resulting solution was stirred vigorously. Then 2 ml of water and 0.5 ml of acetic acid (50%) were added to another 80 ml of ethanol to make an ethanol-water-acetic acid solution. The latter solution was slowly added to the $Ti(O-Bu)_4$-ethanol solution under vigorous stirring. When the resulting mixture turned to a sol, the bismuth nitrate solution was added drop-by-drop. The resulting transparent colloidal suspension was stirred for 1 h and was aged for 2 d until the formation of a gel. The gel was dried at 70 ^{o}C $in\ vacuo$ and then ground. The resulting powder was calcined at 500 ^{o}C for 4 h. A TiO_2 sample was also prepared by the above same procedure without the addition of the bismuth nitrate solution, and this is subsequently referred to as $neat$ TiO_2. The doping concentrations of Bi^{3+} are expressed as wt%.

2.3. Characterization of photocatalysts

The crystalline phases of the synthesized TiO_2 and Bi-TiO_2 catalysts were analyzed by X-ray powder diffraction using a X-ray diffractometer (XRD Philips PW3020) with Cu K_α radiation (λ = 0.154060 nm). An accelerating voltage of 40 kV and an emission current of 30 mA were used. The texture and morphology of the prepared samples were measured by (environmental) scanning electron microscopy (ESEM Phillips XL30), fitted with an EDX accessory. The diffraction pattern and interplanar spacings of the neat and doped catalysts were examined by TEM using a JEOL JEM – 2011 microscope operated at 200 keV. The _____   _____
__   ___
TEM samples were prepared by dispersion in ethanol by sonication and deposition on a carbon film supported on a copper grid. The photoluminescence (PL) emission spectra of the samples were measured at room temperature by two spectrofluorometers (Photon Technology International MD502 and Jobin-Yvon Fluoromax-3) using 325 nm xenon lamp excitation. Low temperature (~10 K) emission spectra of the powder samples of pure TiO_2 and Bi-TiO_2 (1%) were measured at a resolution of 2-4 cm^{-1} using a Panther optical parametric oscillator system pumped by the second harmonic of a Surelite Nd-YAG laser. The crystals were mounted in an

Oxford Instruments closed cycle cryostat. The emission was collected at 90° and passed through an Acton 0.5 m spectrometer equipped with a charge-coupled device. To study the absorption spectra of the photocatalysts, the diffuse reflectance spectra (DRS) of the samples in the wavelength range 250-700 nm was obtained using a spectrophotometer (Shimadzu UV-2101), with MgO as reference. The transmission absorption spectra of TiO_2-Bi (1%) in a KBr disc (0.63 wt%) was recorded in the infrared (by a Nicolet Avatar 360 FTIR instrument) and ultraviolet (by an Agilent 8453 instrument) regions. X-ray photoelectron spectra (XPS) were recorded by a PHI Quantum ESCA Microprobe system using a MgK_{α} excitation source. Calibration of the spectra was done at the C 1s peak of surface contamination taken at 1253.6 eV. The fitting of XPS curves was performed using Multipak 6.0A software.

2.4. *Set up of photocatalytic reactor*

Photodegradation studies of methylparathion were carried out in the photocatalytic reactor system shown in Fig. 1, which consists of a cylindrical borosilicate glass reactor vessel with an effective volume of 250 ml, a cooling water jacket, and a 8 W medium-pressure mercury lamp (Institute of Electric Light Source, Beijing) positioned axially at the center as a 365 nm UV-A light source. The reaction temperature was kept at 25 $^{\circ}$C by cooling water. A special glass frit as air diffuser was fixed at the bottom of the reactor to uniformly disperse air into the solution.

[Fig. 1]

2.5. *Experimental procedure*

In order to investigate the effects of bismuth doping on the photocatalytic activity of TiO_2, the oxidative photodegradation of methylparathion was carried out in the aerated TiO_2 *or* Bi-TiO_2 suspension under UV-A irradiation. The reaction suspensions were prepared by adding 0.25 g of catalyst into 250 ml of aqueous methylparathion solution with an initial concentration of 20 mg l^{-1}. Prior to photoreaction, the suspension was magnetically stirred in a dark condition for 30 min to establish an adsorption/desorption equilibrium condition. The aqueous suspension containing methylparathion and photocatalyst was then UV-A irradiated with constant aeration. At the given time intervals, the analytical samples were taken from the suspension and

immediately centrifuged at 4000 rpm for 15 min, then filtered through a 0.45 μm Millipore filter to remove particles. The filtrate was analyzed by HPLC, DOC and IC for the degree of the methylparathion degradation.

2.6. Analytical methods

The methylparathion concentration was analyzed by a HPLC instrument with a UV-VIS detector (Finnigan Mat Spectra System P4000). In the HPLC analysis, a pinnacle II C18 column (5 μm particle size, 250 mm length and 4.6 mm inner diameter) was employed and mobile phase of acetonitrile/water (7:3 v/v) was used with a flow rate of 0.8 ml min^{-1}. An injection volume of 20 μl was used and the UV detector determined the amount of methylparathion. The DOC concentration was determined by a TOC-analyser (Shimadzu 5000A) equipped with an auto sampler (ASI-5000). The concentrations of the photoreaction products nitrate and sulphate were determined by ion chromatography (IC) using a conductivity detector (Alltech ICM-300 Ion Chromatograph). An Allsep^{TM} (100 mm × 4.6 mm) anion column and mobile phase containing 0.51 mM sodium bicarbonate and 0.54 mM sodium carbonate with a flow rate of 1 ml min^{-1} was used for the determination of nitrate and sulphate.

3. Characterization of photocatalysts

3.1 XRD analysis of TiO$_2$ and Bi-TiO$_2$ photocatalysts

The crystalline quality and crystal structure of TiO$_2$ and Bi-TiO$_2$ samples were examined by XRD and the diffactograms are shown in Fig. 2. It has been reported by several groups [13,14] that sol-gel samples of TiO$_2$ undergo a phase transformation from anatase to rutile phase during sintering treatment. In this study all the samples were sintered at 500 ^{o}C for 2 h in a muffle furnace and the diffractograms in Fig. 2 reveal that all the Bi-TiO$_2$ and pure TiO$_2$ samples possess the anatase phase. No additional peaks are detected.

[Fig. 2]

Based on the XRD results, the crystallite sizes of the TiO_2 and Bi-TiO_2 powders were calculated using the Scherrer equation [17] and were found to be between 16 and 22 nm. The lattice parameters **a** and **c** [18] were measured as 0.38 nm and 0.95 nm in all samples. The doping of up to 2% Bi^{3+} into the TiO_2 lattice therefore does not give significant changes in the diffractograms. Similar conclusions have previously been made by Xu et al. [19] showing that XRD is not sensitive enough to detect such minor changes to the TiO_2 materials.

3.2   ESEM, TEM and EDX analyses of TiO_2 and Bi-TiO_2 photocatalysts

The texture and morphology of the pure TiO_2 sample in comparison with 1%-doped Bi-TiO_2 were also observed by electron microscopy and the typical ESEM micrographs shown in Fig. 3 reveal that both of these two samples were composed of particles with a similar size about 15 nm. Since no obvious particle agglomeration occurred, the large surface area conveys high adsorption abilities of the catalysts. Fig. 4A shows the TEM bright-field image of TiO_2 particles, with average diameter about 22 nm. The inserted image in this figure is their corresponding diffraction pattern. The first four rings correspond to the interplanar distances (in nm) of 0.346, 0.227, 0.186 and 0.168. They are consistent with (101), (103), (004/112) and (200) diffractions from anatase. Fig. 4B shows the bright-field image of Bi-TiO_2 particles. The average diameter of these particles is about 17 nm. Again, the inserted figure is the corresponding diffraction pattern, which can be also indexed as anatase. However, the calculated interplanar distances are slightly larger than for pure TiO_2, as shown in the following for the corresponding first four diffractions (in nm): 0.357, 0.238, 0.192 and 0.173. The TiO_2 lattice is apparently expanded by Bi^{3+} doping.

[Fig. 3]
[Fig. 4]

EDX analysis was carried out for neat and doped TiO_2 using SEM, TEM and ESEM. Fig. 5A shows results from SEM for TiO_2 where only Ti and O are detected. Fig 5B shows the SEM result for 1% Bi^{3+}-doped TiO_2 and the Bi L_α line is observed very weak, and more clearly shown in the inset from TEM-EDX, Fig. 5B. The analytical results from EDX are in reasonable agreement with the nominal wt% of Bi^{3+} doped into TiO_2. EDX elemental maps of samples for

Ti, O and Bi showed homogeneous elemental distributions and no clustering of Bi was detected in the 1%-doped Bi-TiO$_2$ sample.

[Fig. 5]

3.3 XPS and the valence states of TiO$_2$ and Bi-TiO$_2$ photocatalysts

The XPS spectrum shows that there are Ti, O and C on the surface of the neat TiO$_2$, and there are Ti, O, C and Bi on the surface of bismuth doped TiO$_2$. The C arises from the organic precursors for the sol-gel method which are not completely removed during heat treatment. According to the high resolution XPS spectra, the transitions involving the Ti 2p, O 1s, and Bi 4f orbitals are observed. For pure TiO$_2$ and 1% Bi-TiO$_2$, the Ti 2p peaks are narrow with slight asymmetry and have a binding energy of 458.70 eV (full width at half-maximum, FWHM 1.0 eV), showing the presence of Ti^{4+}. There was no evidence for the presence of Ti^{3+} in 1% Bi-TiO$_2$. The O 1s wide peak structure for Bi-TiO$_2$ at 530.79 eV (FWHM 1.36 eV) is at a similar energy to the O 1s electron binding energy for TiO$_2$, where the narrow peak has slight asymmetry with a binding energy of 529.81 eV (FWHM 1.15 eV). Finally, the Bi 4f peaks of Bi-TiO$_2$ consisted of several individual peaks in the region 155-167 eV corresponding to Bi^{3+}.

3.4 Optical absorption properties of photocatalysts

The FTIR spectra of the photocatalysts diluted and pressed in KBr discs show a strong, broad feature between 470 and 690 cm^{-1}, due to Ti-O stretching vibration modes. Weak features are observed at ~3430 and 1630 cm^{-1}, due to adsorbed water. These latter two bands are also present in the KBr disc alone. The UV-visible absorption spectra of Bi-TiO$_2$ samples were measured in the wavelength range 250-800 nm at room temperature using transmission spectra and between 350-500 nm using DRS. The transmission spectrum of a KBr disc of (1%) Bi-TiO$_2$ exhibits an increasing absorption at wavelengths below 500 nm. A clearer comparison of the doped and neat samples is given by DRS (Fig. 6) where it is evident that increasing the %Bi^{3+} doped into the sample gives rise to longer wavelength absorption. Extending the absorption of TiO$_2$ further into the visible region is expected to provide enhanced photocatalytic behaviour. A

brief discussion is now given concerning the reasons for the long wavelength tail in the doped photocatalysts.

[Fig. 6]

According to theory [20], semiconductors absorb light below a threshold wavelength λ_g (the fundamental absorption edge). The band gap energy value of anatase (TiO_2) is about 3.2 eV with the threshold wavelength $\lambda_g = 387.5$ nm. It is well known that intrinsic transitions give sharp increases in absorbance whereas impurity or defect state transitions give absorption tails in semiconductors. An impurity atom changes its local lattice environment, but since the $6s^2$ configuration Bi^{3+} ion (ionic radius 103 pm) is unable to directly substitute the $4s^0$ Ti^{4+} ion (ionic radius 61 pm) using a "soft" chemical method of preparation, a new phase is formed. An analogous case has been observed when the lanthanide ion Er^{3+} is doped into α-Al_2O_3 [21] where the host ion size is also much smaller, so that new compounds are formed, with $ErAlO_3$ being formed at lower dopant ion concentrations of Er^{3+}, rather than $Er_3Al_5O_{12}$. Several compounds have been well characterized in the Bi^{3+}-TiO_2 case: $Bi_2Ti_2O_7$ [22], $Bi_4Ti_3O_{12}$ [23,24] and $Bi_{12}TiO_{20}$ [25]. The first of these comprises disordered $(Bi_2O)^{4+}$ tetrahedral nets interpenetrating with corner-sharing $(Ti_2O_6)^{4-}$ octahedra [26]; the second consists of three $(Bi_2Ti_3O_{10})^{2-}$ layers sandwiched between two $(Bi_2O_2)^{2+}$ layers [19]; whereas the third comprises $(TiO_4)^{4-}$ tetrahedra and a Bi-O polyhedral network [25]. All compounds exhibit two characteristic features. First, the band gap is reduced from that of TiO_2, with the energy band assumed to be between the top of the (lone pair) Bi^{3+} 6s band and the bottom of the Ti^{4+} 3d band [25]. Thus the absorption spectra extend to longer wavelengths so that lower energy photons can be absorbed for photoreaction. Second, the positively-charged Bi-O polyhedra can function as electron sinks, which has repercussions for the photoluminescence and photocatalytic properties.

3.5   PL spectra of the photocatalysts

The PL spectra are useful to disclose the efficiency of charge carrier trapping, migration and transfer, and to understand the nature of electron-hole pairs in semiconductor particles since PL emission results from the recombination of free carriers. In this study, the 325 nm excited

room temperature PL spectra of all pressed-powder samples were examined in the range of 350-550 nm. The results (not shown here) indicated that the luminescence intensity of neat TiO_2 (λ_{em}(max) $\sim$ 388 $\pm$ 10 nm; FWHM $\sim$ 75 nm) was substantially quenched by the doping of Bi^{3+}. The relative intensity of the 0.3% and 1% Bi^{3+}-doped samples was $\sim$0.7 of that of undoped samples. No significant band shifts were observed. Thus Bi^{3+} doping of TiO_2 hinders free carrier recombination under irradiation.

The emission spectra of neat TiO_2 and (1.0%) Bi-TiO_2 were also recorded at 10 K under 355 nm laser excitation and the results shown in Fig. 7 differ considerably from those at room temperature. First, the neat TiO_2 emission band is red-shifted to 542 nm (2.3 eV). Furthermore, the quenching of emission by Bi^{3+} is more pronounced and the Bi^{3+}-doped sample emits at a slightly longer wavelength. The low energy emission band in the neat TiO_2 sample resembles the $\sim$530 nm emission band reported for TiO_2:Er^{3+} under 325 nm excitation at 20 K. The latter has been assigned to the reduction of Ti^{4+} to Ti^{3+} after H_2O adsorption [27]. However, this hypothesis requires further confirmation since the emission could otherwise be due to self-trapped exciton states in TiO_2 [28]. It is clear however that Bi^{3+} again acts as a trapping centre.

[Fig. 7]

4. Photocatalytic degradation of methylparathion

4.1   *Photocatalyst activity for the degradation of methylparathion*

In order to determine the photocatalytic activity of Bi-TiO_2 and find out the optimum content of Bi impurity, a set of experiments for methylparathion degradation under UV-A irradiation was carried out in aqueous suspension with either TiO_2 or different Bi-TiO_2 catalysts with a Bi content between 0.3% and 2%, and the experimental results are shown in Fig. 8. The experiments demonstrated that methylparathion was degraded by more than 95% within 120 min for all catalysts including pure TiO_2. However, the Bi-TiO_2 catalysts attained faster degradation rates than the neat TiO_2 catalyst. For example, the experiment using 1.5% Bi-TiO_2 achieved a complete degradation of methylparathion at 90 min. It was found that pseudo-first-order kinetics was obeyed for the photocatalytic degradation of methylparathion as illustrated in Fig. 8. The

calculated first-order kinetic constants are listed in Table 1 and show maximum values in the range of Bi^{3+} content between 0.7 and 1.5 wt%. It is well-known that the photocatalytic mechanism of TiO_2 involves electron-hole production, with the separated electrons and holes generating reactive radical species such as $O^{2-}\cdot$ and $\cdot OH$, respectively. Thus from the kinetic results it is clear that $Bi\text{-}TiO_2$ at intermediate doping concentrations functions more effectively as a separation center. Presumably the reduced efficiency at the highest dopant ion concentration (2%) is due to the formation of Bi^{3+} clusters.

[Fig. 8]

The reactive radicals formed in the photocatalytic process further react with organic and inorganic compounds adsorbed on TiO_2 and oxidize or reduce them. Generally speaking, the photocatalytic activity of TiO_2 mainly depends upon three factors: (1) the electron-hole generation capacity; (2) the separation efficiency of the photogenerated charge pair; and (3) the charge transfer efficiency of holes and electrons to compounds adsorbed on TiO_2. The yield of the photogenerated electron-hole pair first depends upon the intensity of incident photons with energy exceeding or equaling to the TiO_2 band gap energy. Our results indicate that $Bi\text{-}TiO_2$ photocatalyst is superior to neat TiO_2 for methylparathion degradation since the degradation rate is almost doubled. As mentioned above, the most effective photocatalysts are in the regime of 0.7-1.5% Bi^{3+} doping. This efficiency is ascribed to process (2) in which the Bi-O polyhedral centres act as traps for photogenerated electrons and deter the pair recombination process.

4.2   *Effect of pH on the degradation of methylparathion*

The effect of pH upon the photocatalytic degradation of methylparathion by $Bi\text{-}TiO_2$ was investigated by performing the degradation study in the initial pH range of 2 to 10 for 1% Bi^{3+} doping, with the initial concentrations (C_0) of methylparathion 20 mg l^{-1} and catalyst 1 g l^{-1}. The experimental results are shown in Fig. 9.   A higher degradation rate and adsorption were observed at low pH values, with a monotonic rate constant decrease from pH 2 ($k \sim 5 \times 10^{-2}$ min^{-1}) to pH 10.0 ($k \sim 3.5 \times 10^{-2}$ min^{-1}). The amphoteric behaviour of many metal oxides changes the surface charge properties of the catalyst when the pH changes. For $Bi\text{-}TiO_2$, increasing the solution pH diminished the adsorption of methylparathion. The zero-point charge pH_{zpc} is 6.8 for

TiO$_2$ particles (Degussa) [29]. In the Bi-TiO$_2$ system, TiO$_2$ is more positively charged in an acidic medium (pH < 6.8) than in an alkaline medium (pH > 6.8) based upon the zero point charge. Hence, at lower pH methylparathion, which has electronegative centres (N and S), can have enhanced adsorption on the catalyst surface. This effect acts to increase the degradation of methylparathion at lower pH. It was also observed from mass balance experiments performed in the dark that very little methylparathion is actually adsorbed onto the catalyst. The rate of photodegradation therefore has the bottleneck of adsorption. In this study, all the experiments with different initial pH values were conducted without a pH control. It was found that pH decreased during the photocatalytic degradation of methylparathion. For example, the reaction solution with an initial pH 7 was run for 120 min with a final pH 3.6. These results indicate that the products of methylparathion degradation contain a certain amount of acidic compounds: either organic acids such as oxalic acid, acetic acid and formic acid or inorganic acids such as sulphuric acid and nitric acid, according to a pathway of methylparathion degradation proposed by Vlyssides et al. [2].

[Fig. 9]

4.3   Mineralization of methylparathion

To study the mineralization of methylparathion in this photocatalytic reaction, a set of experiments of methylparathion degradation with an initial concentration of 20 mg l^{-1} (DOC = 7.3 mg l^{-1}) was carried out using different photocatalysts and samples were collected at suitable time intervals for up to 120 min, and then analyzed for DOC concentration. The experimental results are shown in Fig. 10. The DOC removals after 120 min are given in parentheses for the various photocatalysts: neat TiO$_2$ (21%), 0.3% Bi-TiO$_2$ (39%), 0.5% Bi-TiO$_2$ (42%), 0.7%Bi-TiO$_2$ (53%), 1% Bi-TiO$_2$ (61%), 1.5% Bi-TiO$_2$ (58%), and 2.0% Bi-TiO$_2$ (46%). These results indicate that the doping regime between 0.7% and 1.5% of Bi^{3+} achieved the highest percentage of DOC removal.

[Fig. 10]

In order to elucidate the mineralization pathways for the degradation of methylparathion, a detailed investigation was carried out using 1% Bi-TiO$_2$ for 180 min. During the reaction, samples were collected and analyzed for concentrations of methylparathion, DOC, nitrate ion, and sulphate ion. The normalized experimental results are shown in Fig. 11. It can be seen that methylparathion almost disappeared at 90 min. However, although the DOC concentration in the solution decreased significantly during the photoreaction from the initial value of 7.3 mg l^{-1}, 47% of the initial DOC still remained. After 120 min, methylparathion was completely degraded, whereas DOC had 38% leftover. It is clear that the disappearance of the reactant was considerably faster than the mineralization process. The experimental results also confirm that the decomposition of methylparathion proceeded by a nitrate and sulphate release pathway. After 180 min, conversion of nitrogen (N) and sulphur (S) from organic forms into inorganic products was achieved by 68% and 84%, respectively, whereas the conversion of carbon (C) was by 74% with 26% of DOC remaining. These results indicate that the conversion of carbon, nitrogen and sulphur was ranked from high to low as S > C > N during this photocatalytic reaction. The pathway proposed by Vlyssides et al. [2] also illustrates the sequencing steps of methylparathion degradation reaction, in which sulphate formation occurs at an earlier stage than nitrate formation.

[Fig. 11]

5.   Conclusions

A series of bismuth-deposited titania samples were prepared, well-characterized, and then employed for the photodegradation of methylparathion under UV-A radiation. The photocatalytic degradation of methylparathion in aqueous solutions was further promoted by the Bi-TiO$_2$ photocatalysts, compared with neat TiO$_2$ alone. The doped bismuth was shown to be present in the 3+ oxidation state by XPS, and to exist in pores or on the surface of the TiO$_2$ as regions of positive sites comprising Bi-O polyhedra. The optimal content of Bi^{3+} doping for photocatalysis was in the regime between 0.7 and 1.5%. The ability of the Bi-O sites to act as electron traps was not only illustrated in the photocatalysis experiments but also in the photoluminescence study. In summary, it has been demonstrated that methylparathion was

effectively degraded in aqueous Bi-TiO$_2$ suspension to an extent of 97% within 120 min, whilst DOC was also converted into CO$_2$ with the high proportion of up to 62%. This study confirms the potentialities of heterogeneous photocatalysis to decontaminate wastewaters containing organic pollutants, which are often toxic for bacteria in biological treatments. The present findings can be valuable in designing in-situ treatment of pesticide-contaminated water and wastewater.

Acknowledgements

References

[1] FAO Pesticide Disposal Series. Baseline study on the problem of obsolete pesticide stocks; Rome, 2000.

[2] A. Vlyssides, E.M. Barampouti, S. Mai, D. Arapoglou, A. Kotronarou, Environ. Sci. Technol. 38 (2004) 6125.

[3] J.J. Pignatello, Y. Sun, Water Res. 29 (1995) 1837.

[4] T. Chen, R. Dong, W. Lei, Water Res. 37 (1998) 187.

[5] A. Kotronarou, G. Mills, M.R. Hoffmann, J. Phys. Chem. 95 (1991) 3630.

[6] M. Zeinali, A. Torrents, Environ. Sci. Technol. 32 (1998) 2338.

[7] A. Fujishima, T.N. Rao, D.A. Tryk, J. Photochem. Photobiol. C. Photochem. Rev.1 (2000) 1.

[8] X.Z. Li, F.B. Li, Environ. Sci. Technol. 35 (2001) 2381.

[9] H. Yamashita, Y. Ichihashi, M. Anpo, M. Hashimoto, C. Louis, M. Che, J. Phys. Chem. B. 100 (1996) 16041.

[10] Z.B. Zhang, C.C. Wang, R. Zakaria, J.Y. Ying, J. Phys. Chem. B. 102 (1998) 10871.

[11] S. Rengaraj, X.Z. Li, International J. Environ. Poll. (2005) (in press).

[12] A. Mills, R.H. Davies, D. Worsley, Chem. Soc. Rev. 22 (1993) 417.

[13] A.L. Linsebigler, G.Q. Lu, J.T. Yates, Chem. Rev. 95 (1995) 735.

[14] J. Engweiler, J. Harf, A. Baiker, J. Catalysis 159 (1996) 259.

[15] J.M. Hermann, H. Tahiri, Y. Ait-Ichou, G. Lassaletta, A.R. Gonzalez-Elipe, A. Fernandez, Appl. Catal. B Environ. 13 (1997) 219.

[16] I.R. Bellobono, A. Carrara, B. Barni, A. Gazzotti, J. Photochem. Photobiol A., 84 (1994) 83.

[17] J. Liu, J.C. Yu, D. Lo, S.K. Lam, J. Catal. 183 (1999) 368.

[18] L.R. Feng, C.J. Lu, F.L. Qiu, Acta Chimica Sinica. 60 (2002) 463.

[19] X.H. Xu, M. Wang, Y. Hou, W.F. Yao, D. Wang, H. Wang, J. Mat. Sci. Lett. 21 (2002)1655.

[20] N. Serpone, E. Pelizzetti, In Photocatalysis: Fundamentals and Application, Edition I; Wiley-Interscience: New York; 1989. p. 123.

[21] P.A. Tanner, K.L. Wong, Y. Liang, Chem. Phys. Lett. 399 (2004) 15.

[22] W.F. Yao, X.H. Xu, H. Wang, J.T. Zhou, X.N. Yang, Y. Zhang, S.X. Shang, B.B. Huang., Appl. Cat. B Environ. 52 (2004) 29.

[23] P. Pookmanee, P. Uriwilast, S. Phanichpant, Ceramics Intern. 30 (2004) 1913.

[24] W.F. Yao, H. Wang, X.H. Xu, S.X. Shang, Y. Hou, Y. Zhang, M. Wang, Mater. Lett. 57 (2003) 1899.

[25] W.F. Yao, H. Wang, X.H. Xu, X.F. Cheng, J. Huang, S.X. Shang, X.N. Yang, M. Wang, Appl. Catal. A General 243 (2003) 185.

[26] A.L. Hector, S.B. Wiggin, J. Solid St. Chem. 177 (2004) 139.

[27] S. Komuro, T. Katsumata, H. Kokai, T. Morikawa, X. Zhao, Appl. Phys. Lett. 81 (2002) 4733.

[28] V. Kiisk, I. Sildos, O. Sild, J. Aarick, Opt. Mater. 27 (2004) 115.

[29] J.C. Zhao, T.X. Wu, K.Q. Wu, K. Oikawa, H. Hidaka, N. Environ. Sci. Technol. 32 (1998) 2394.

Table 1.

First-order kinetic constants of methylparathion photodegradation by Bi-TiO$_2$ (Initial concentration, C$_o$ = 20 mg l^{-1})

Photocatalyst	Kinetic constant, k (min^{-1})	Coefficient of determination, R^2
Pure TiO$_2$	3.8×10^{-2}	0.9571
0.3% Bi-TiO$_2$	3.3×10^{-2}	0.9937
0.5% Bi-TiO$_2$	3.7×10^{-2}	0.9724
0.7% Bi-TiO$_2$	5.3×10^{-2}	0.9953
1.0% Bi-TiO$_2$	4.8×10^{-2}	0.9990
1.5% Bi-TiO$_2$	5.6×10^{-2}	0.9975
2.0% Bi-TiO$_2$	4.1×10^{-2}	0.9914

Figure Captions

Fig. 1. The schematic diagram of the photoreactor system (1. air; 2. water; 3. UV-A lamp; 4. timer; 5. stirrer; 6. quartz jacket).

Fig. 2. XRD diffractograms of (a) TiO_2 and (b)-(d) Bi-TiO_2. The structure corresponds to anatase (A) [15,16].

Fig. 3. ESEM micrographs of two photocatalysts: (A) TiO_2 and (B) 1% Bi-TiO_2.

Fig. 4. TEM micrographs of (A) TiO_2 and (B) 1% Bi-TiO_2. The inserted figures indicate the diffraction patterns of the anatase phase.

Fig. 5. SEM-EDX of two photocatalysts (A) TiO_2 and (B) 1% Bi-TiO_2. The inset in (B) shows the TEM-EDX result for (B) at higher sensitivity.

Fig. 6. Diffuse reflectance UV-visible spectra of neat and Bi^{3+}-doped TiO_2 at room temperature.

Fig. 7. The PL spectra of neat TiO_2 and 1% Bi^{3+}-doped TiO_2 photocatalysts in the range of 440-740 nm at 10 K. The breaks in the curves are artifacts due non-overlap of the window edges of the charge-coupled device detector.

Fig. 8. Kinetic fits for the degradation of methylparathion by TiO_2 and Bi-TiO_2. (Initial concentration of methylparathion 20 mg l^{-1}; pH 3.4; catalyst 1 g l^{-1}).

Fig. 9. Effect of pH on the degradation of methylparathion by Bi-TiO_2. (Initial concentration of methylparathion 20 mg l^{-1}; catalyst 1 g l^{-1})
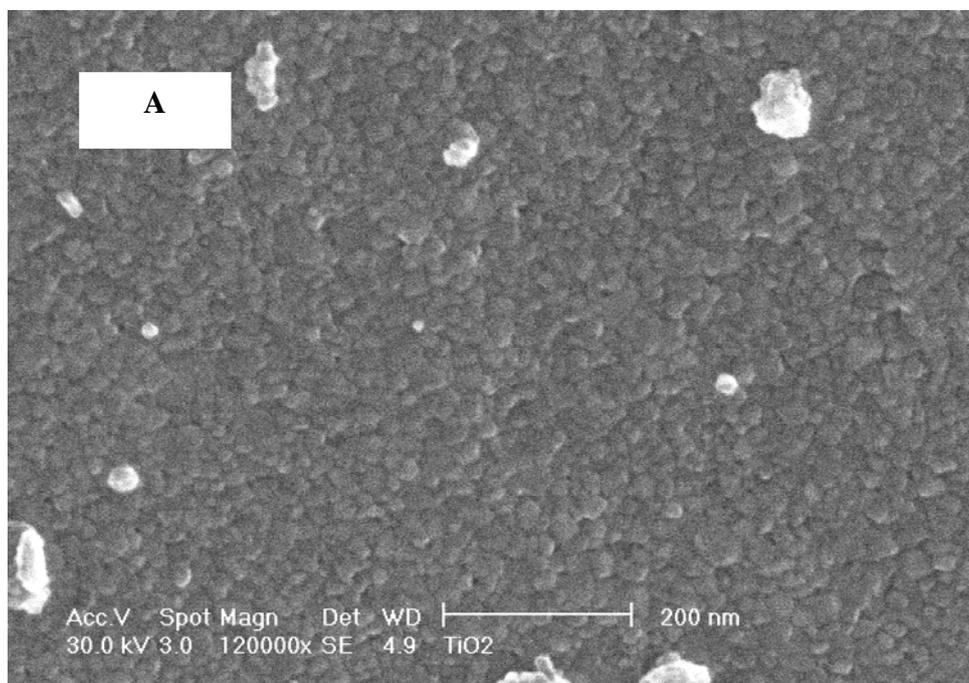
Fig. 10. DOC removals during methylparathion degradation using different catalysts

Fig. 11. Time change of normalized concentration of methylparathion, DOC, sulphate and nitrate in the mineralisation of methylparathion. (Initial concentration of methylparathion 20 mg l^{-1}; catalyst 1 g l^{-1}).

Fig. 1.

Fig. 2.

Fig. 3.

A

100 nm

B

100 nm
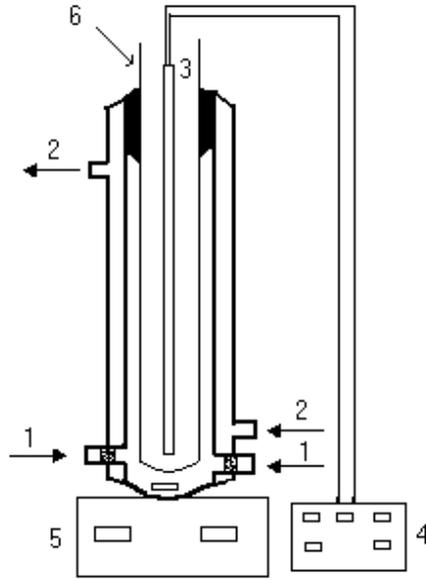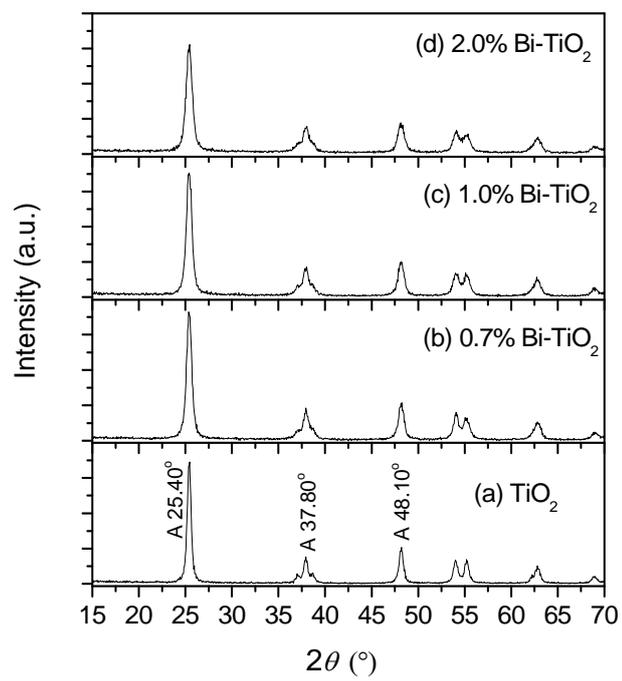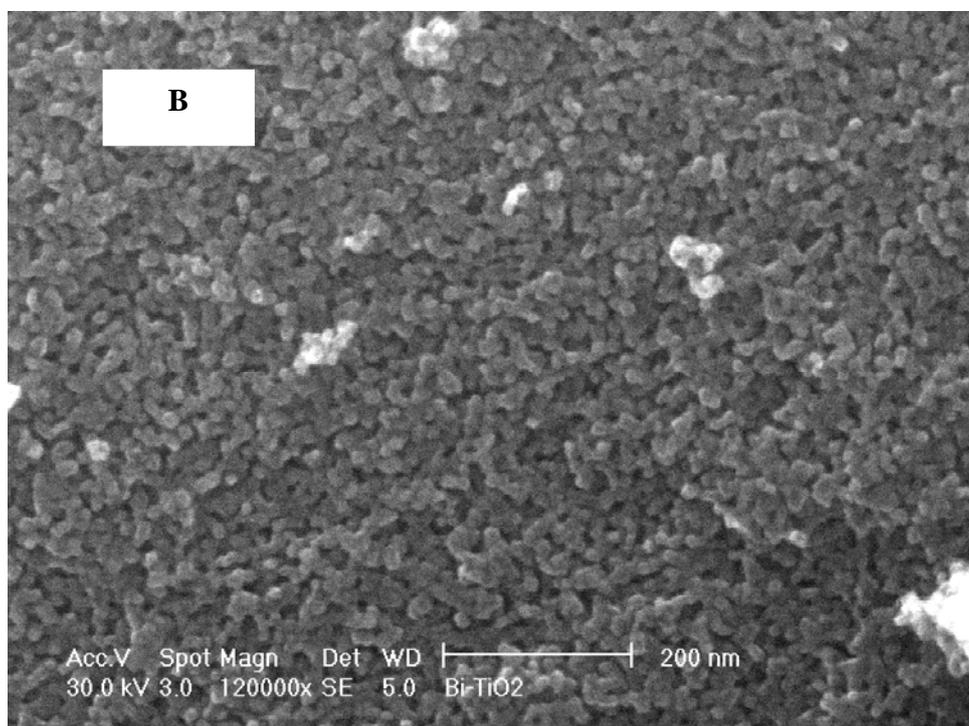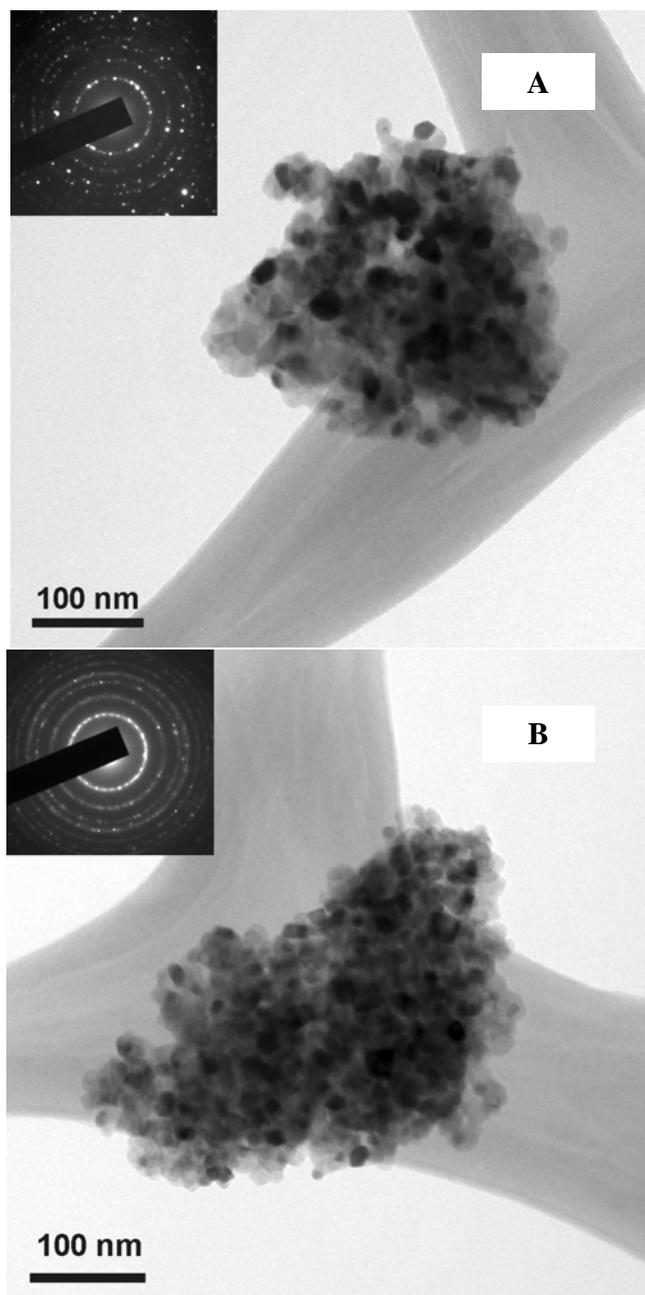
Fig. 4.
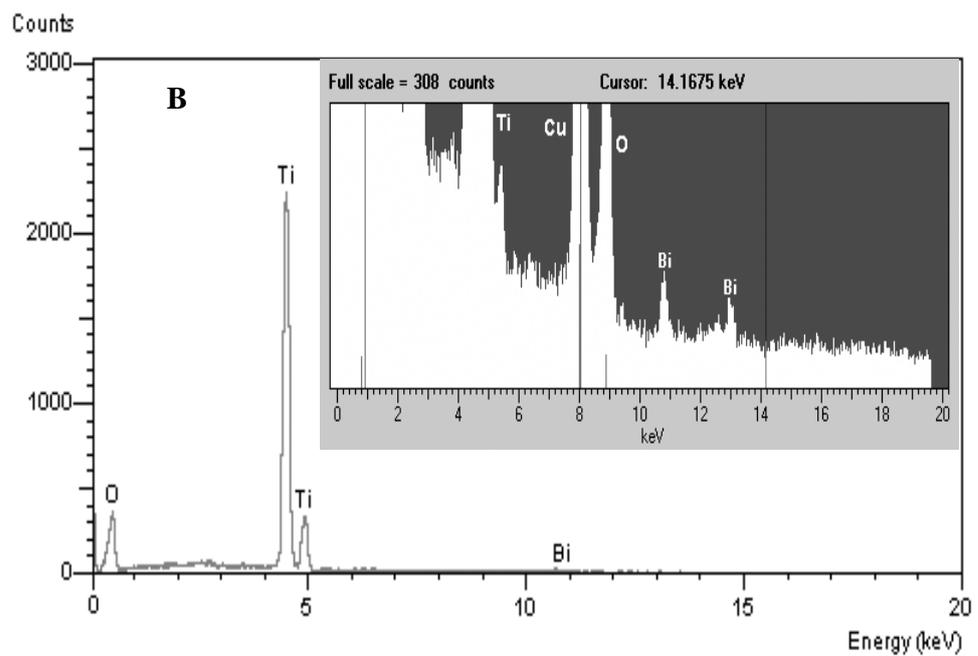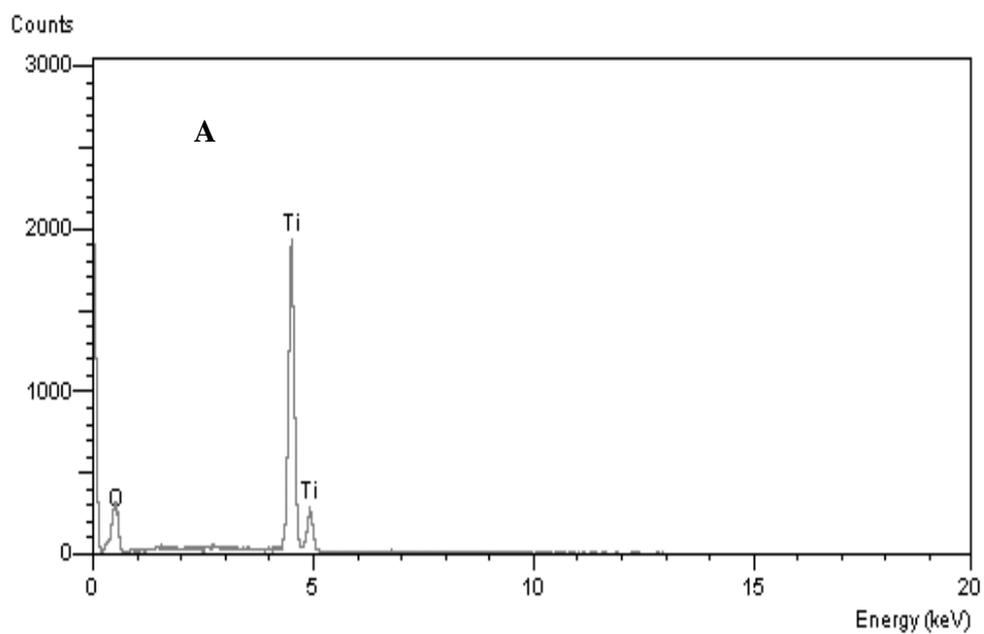
Fig. 5
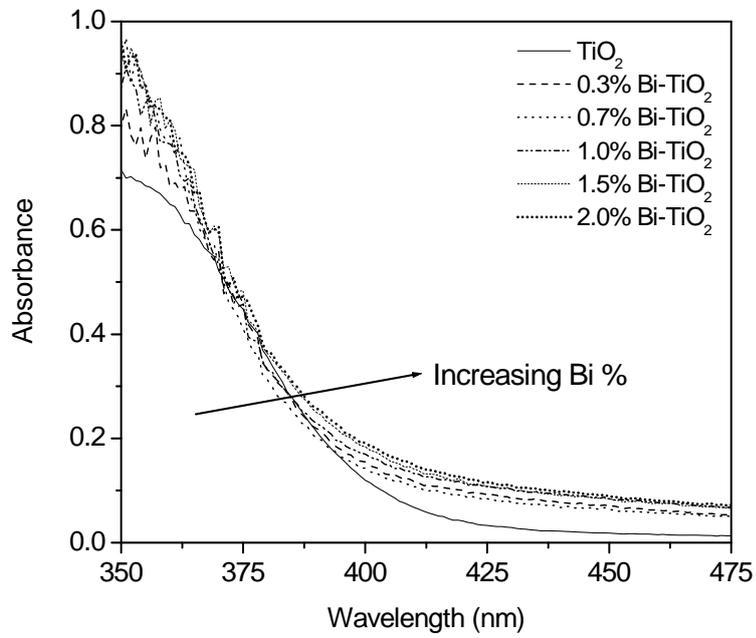
Fig. 6.
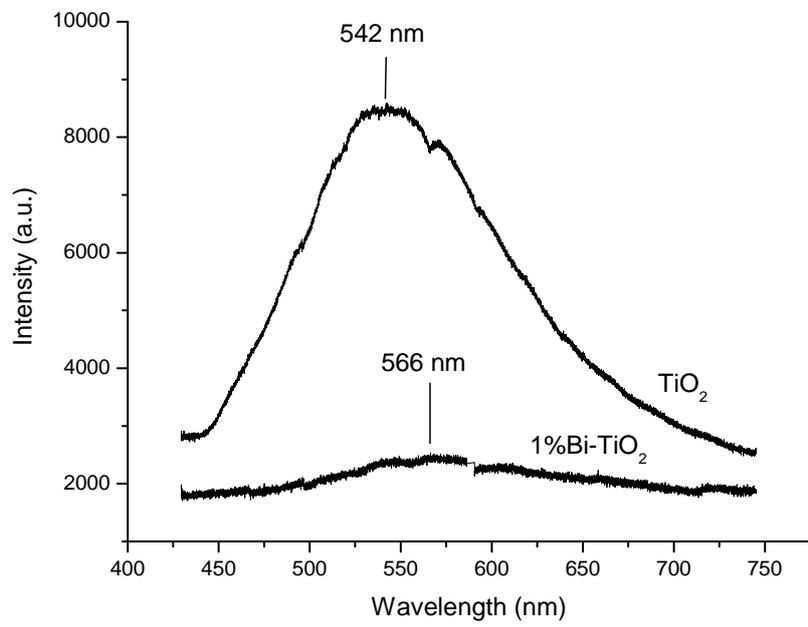
Fig. 7

Fig. 8

Fig. 9

Fig. 10

Fig. 11